Frequency-dependent critical viscosity of a classical fluid

Jayanta K. Bhattacharjee
Institut fur Festkörperforschung der Kernforschungsanlage, D-5170 Jülich 1, West Germany

Richard A. Ferrell
Center for Theoretical Physics of the Department of Physics and Astronomy, University of Maryland, College Park, Maryland 20742

(Received 14 September 1982)

Just as a finite temperature shift brings the critical viscosity down from its diverging critical-point behavior, a finite frequency produces a similar reduction. We compute in detail the frequency-temperature scaling function to single-loop order and apply it to the problem of critical diffusion. We also present detailed numerical estimates of the "rolloff" to be expected in direct experimental viscosity measurements carried out at finite frequencies.

I. INTRODUCTION

As the critical point of a classical fluid is approached, a weak but nonetheless striking divergence sets in in the hydrodynamic viscosity. This effect has been extensively studied experimentally for both the liquid-vapor phase transition of a single-component fluid and for the consolute point of a binary mixture. The dominant features of the effect are well described by the decoupled-mode theory to single-loop order.[1,2] Two years ago[3] we pointed out an interesting modification that is predicted by the decoupled-mode theory for the case that the viscosity is measured at a finite frequency ω. This makes the approach to the critical point qualitatively different, as soon as the characteristic order-parameter relaxation rate drops below ω. The system is then no longer in equilibrium, and the singularity in the hydrodynamic viscosity η_s is blunted. Instead of

$$\eta_s(\kappa) \propto \kappa^{-z_\eta} , \tag{1.1}$$

where κ^{-1} is the correlation length and z_η is the small critical viscosity exponent, the temperature- and frequency-dependent viscosity $\eta(\kappa,\omega)$ acquires at the critical point the frequency dependence

$$\eta(0,\omega) \propto \omega^{-z_\eta/(3+z_\eta)} . \tag{1.2}$$

The general $\kappa-\omega$ dependence can be written as

$$\eta(\kappa,\omega)=\eta_s(\kappa)S^{-z_\eta/(3+z_\eta)} \tag{1.3}$$

in terms of the scaling function $S(z)$ of the scaled frequency

$$z=\frac{-i\omega}{2\kappa^2 D_s(\kappa)} , \tag{1.4}$$

where $D_s(\kappa) \propto \kappa^{1+z_\eta}$ is the critical diffusion coefficient in the hydrodynamic limit.

In order to illustrate qualitatively the behavior of $S(z)$ we used[3] the single-factor approximant

$$\bar{S}_1(z) \simeq 1+B_0 z , \tag{1.5}$$

where B_0 is a coefficient specified below. The purpose of this paper is to point out that for quantitative purposes a much improved and reasonably satisfactory fit to $S(z)$ is provided by the somewhat more elaborate three-parameter, two-factor approximant

$$\bar{S}_2(z) \simeq (1+B_1 z)^{\beta}(1+B_2 z)^{1-\beta} . \tag{1.6}$$

Section II is devoted to a determination of the three parameters of Eq. (1.6). In Sec. III we make use of the spectral function for comparing Eq. (1.6) with the exact, but rather unwieldy, expression for $S(z)$ that is obtained in the Appendix. In Sec. III we also obtain an alternative analytic approximant for $S(z)$. In Sec. IV we apply Eq. (1.6) to the problem of critical diffusion in a classical fluid. Section V constitutes a brief summary.

II. FREQUENCY DEPENDENCE

Because of $z_\eta \ll 1$ we can linearize Eq. (1.3) in z_η and work with $\ln S(z)$. The single-loop decoupled-mode expression for $\ln S(z)$ is

$$\begin{aligned}\ln S &= 3\int_0^\infty \frac{dp\,p^6}{(p^2+1)^2}\left[\frac{1}{p^2(p^2+1)^{1/2}} - \frac{1}{z+p^2(p^2+1)^{1/2}}\right] \\ &= 3z\int_0^\infty \frac{dp\,p^4}{(p^2+1)^{5/2}}\left[\frac{1}{z+p^2(p^2+1)^{1/2}}\right] \\ &= \frac{3\pi}{16}z-\frac{8}{5}z^2+\cdots ,\end{aligned} \tag{2.1}$$

 ©1983 The American Physical Society

where the last line exhibits the low-frequency behavior. It is worthwhile to study both the low- and high-frequency behavior of S with the goal of developing an approximant for S in the form of Eq. (1.6). This is what we now proceed to do in this section.

The remainder in Eq. (2.1) is of higher order than z^2 but is not expressible as a Taylor series with integer powers. Substitution of Eq. (1.5) into Eq. (2.1) and identifying the terms linear in z yields

$$B_0=\tfrac{3}{16}\pi=0.589\ , \tag{2.2}$$

the value used in Ref. 3. But Eqs. (1.5) and (2.2) give an accurate representation of $S(z)$ only in the range of small z. In the opposite limit for $z\gg 1$ Eq. (2.1) becomes

$$\ln S\simeq\int_0^\infty dp\left[\frac{3p^4}{(p^2+1)^{5/2}}-\frac{3p^2}{z+p^3}\right]$$
$$=\ln z+3\ln 2-4=\ln(B_\infty z)\ , \tag{2.3}$$

where

$$B_\infty=8e^{-4}=0.146\ . \tag{2.4}$$

Thus we see that the coefficient of z in Eq. (1.5) has to be regarded as a z-dependent quantity which undergoes a considerable decrease in passing from the low-z to the high-z region. This is effectively what is accomplished in Eq. (1.6).

The three parameters of Eq. (1.6) are determined by identifying the linear and quadratic terms of $\ln S$ with those of Eq. (2.1). The required third piece of information is obtained by comparing the $z\gg 1$ behavior of $\ln S$ with that of Eq. (2.3),

$$\beta B_1+(1-\beta)B_2=\tfrac{3}{16}\pi\ , \tag{2.5}$$

$$\beta B_1^2+(1-\beta)B_2^2=\tfrac{8}{5}\ , \tag{2.6}$$

$$\beta\ln B_1+(1-\beta)\ln B_2=3\ln 2-4\ . \tag{2.7}$$

The solution of these equations is facilitated by the fact that B_2 has only a small effect in Eq. (2.5), is completely negligible in Eq. (2.6), and dominates in Eq. (2.7). Solution by iteration gives

$$\beta B_1=0.526\ , \tag{2.8}$$

so from Eq. (2.6) we obtain

$$\beta=0.173 \tag{2.9}$$

and

$$B_1=3.04\ . \tag{2.10}$$

Substitution into Eq. (2.7) yields

$$B_2=0.0778\ . \tag{2.11}$$

The resulting log-log plot of S vs z is shown by the dashed curve of Fig. 1. The solid curve shows the results of numerical integration, while the asymptotic behavior specified by Eqs. (2.3) and (2.4) is exhibited by the dot-dash straight line. A comparison of the two curves in Fig. 1 confirms that Eqs. (2.9)–(2.11) provide a reasonably accurate representation of $\ln S$ with the maximum error at intermediate values of z of -0.2.

We have noted that for some purposes we can use the single-factor approximant

$$\bar{S}_1(z)\simeq 1+\tfrac{1}{4}z\ , \tag{2.12}$$

which crosses the dashed and solid curves at $z=3$ and 12, respectively. This is of the general form of Eq. (1.5) but with a choice of coefficient in between B_0 and B_∞. Equation (2.12) gives a satisfactory fit to $S(z)$ in the intermediate region at the cost of an error of -0.1 in the low-frequency region. The error changes sign at $z\simeq 10$ and increases monotonically in the high-frequency region, reaching 0.5 in the limit $z\to\infty$. To this accuracy, Fig. 1 of Ref. 3 still describes the expected scaling behavior for a finite frequency measurement of the viscosity, with, however, an adjustment of the frequency scale by the factor $4B_0=3\pi/4\simeq 2.4$. A more precise result is obtained according to Eqs. (1.6) and (2.9)–(2.11) by making scale changes in Fig. 1 of Ref. 3 of $4B_{1,2}$ and superposing the results with weights of β and $1-\beta$, respectively.

In applying Eq. (1.3) to complex or purely imaginary values of $z=-i\Omega$ it should be noted that $\ln S$ becomes itself complex. Im $\ln S$ is, however, bounded, so that by virtue of $z_\eta\ll 1$, its exponentiation is not necessary. It follows, to $O(z_\eta)$, that the scaling factor in Eq. (1.3) can be put into the simplified form

$$S^{-z_\eta/(3+z_\eta)}\simeq\exp(-\tfrac{1}{3}iz_\eta\,\mathrm{Im}\ln S)$$
$$\times\exp(-\tfrac{1}{3}z_\eta\,\mathrm{Re}\ln S)$$
$$\simeq(1-\tfrac{1}{3}iz_\eta\,\mathrm{Im}\ln S)$$
$$\times\exp(-\tfrac{1}{3}z_\eta\,\mathrm{Re}\ln S)\ . \tag{2.13}$$

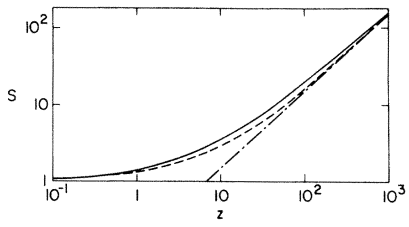

FIG. 1. Scaling function $S(z)$ vs reduced frequency $z=-i\omega/\gamma$. Solid and dashed curves show the exact function and the two-factor approximant $\bar{S}_2$, respectively. Dot-dashed straight line is the high-frequency asymptote.

As discussed in Ref. 3, the effective viscosity that is measured experimentally is in fact proportional to the sum of the real and imaginary parts, i.e.,

$$(\mathrm{Re}+\mathrm{Im})S^{-z_\eta/(3+z_\eta)} \simeq (1-\tfrac{1}{3}z_\eta \mathrm{Im}\ln S) \times \exp(-\tfrac{1}{3}z_\eta \mathrm{Re}\ln S) . \tag{2.14}$$

It is convenient to divide Eq. (2.14) by the critical point value of $\mathrm{Re}S^{-z_\eta/(3+z_\eta)}$ to give

$$(1-\tfrac{1}{3}z_\eta \mathrm{Im}\ln S)\exp\{\tfrac{1}{3}z_\eta[\ln(B_\infty \Omega)-\mathrm{Re}\ln S]\} \simeq \exp(\tfrac{1}{3}z_\eta H) , \tag{2.15}$$

where

$$H(\Omega)=\ln B_\infty \Omega - \mathrm{Re}\ln S - \mathrm{Im}\ln S . \tag{2.16}$$

III. SPECTRAL FUNCTION

A. Dimensional variation

An integration of Eq. (2.1) in closed form is presented in the Appendix. But the resulting expression is so cumbersome as to have limited practical application. We therefore follow a different tack in this section. It is evident from Eq. (2.1) that the scaling function can be expressed in terms of the subtraction

$$\ln S(z)=J(0)-J(z) , \tag{3.1}$$

where

$$J(z)=3\int_0^{q_D} \frac{dp\,p^6}{(1+p^2)^2}\frac{1}{z+p^2(1+p^2)^{1/2}} . \tag{3.2}$$

q_D is the Debye cutoff, in units of k. With the variable change

$$s=p^2(1+p^2)^{1/2} , \tag{3.3}$$

Eq. (3.2) can be rewritten as

$$J(z)=\int_0^{q_D^3} ds \frac{f(s)}{s+z} , \tag{3.4}$$

corresponding to a continuous distribution of purely relaxational contributions. The weighting function, or spectral function

$$f(s)=3\frac{p^6}{(1+p^2)^2}\frac{dp}{ds} \tag{3.5}$$

is shown by the solid curve in Fig. 2.

Any given approximation to $J(z)$, and thus to $S(z)$, can be examined and judged according to the corresponding approximation to the spectral function. In this light, the single-factor approximant has to be judged to be quite crude, corresponding as it does to the single-step spectral function

$$\bar{f}_1(s)=\begin{cases}0 , & 0\le s<B_0^{-1}\\ 1 , & B_0^{-1}\le s\end{cases} \tag{3.6}$$

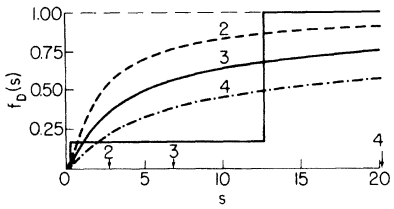

FIG. 2. Spectral function $f_D(s)$ vs s for spatial dimensionality $D=2$, 3, and 4. Arrows show the corresponding effective low-frequency cutoffs. Two-step function is the spectral function for the two-factor approximant $\bar{S}_2$.

The two-factor approximant of Eq. (1.6) is clearly better in that its two-step spectral function is a somewhat more realistic representation of the continuous monotonic function of Eq. (3.5). The steps at $s=B_{1,2}^{-1}$ are of height β and $1-\beta$, respectively. Using the values of β, B_1, and B_2 from Eqs. (2.9)–(2.11), we obtain the two-step spectral function $\bar{f}_2(s)$, as shown in Fig. 2. $\bar{f}_2(s)$ is an improvement over $\bar{f}_1(s)$ in that the small step at $s=B_1^{-1}=0.3$ simulates the threshold behavior of $f(s)$. However, $\bar{f}_2(s)$ deviates significantly from $f(s)$ in the intermediate-frequency region, as is directly evident in Fig. 2 and as is also indirectly manifested by the error of -0.2 in Fig. 1. This difference is sufficient to warrant the further improvement that we now proceed to describe.

In order to obtain an improved representation of S it is useful to generalize the single-loop integral of Eq. (3.2) to arbitrary spatial dimensionality D. Thus

$$J_D(z)=D\int_0^{q_D} \frac{dp\,p^{D+3}}{(1+p^2)^2}\frac{1}{z+p^2(1+p^2)^{D/2-1}} \tag{3.7}$$

and

$$\ln S_D(z)=J_D(0)-J_D(z) . \tag{3.8}$$

For $D=3$, Eqs. (3.7) and (3.8) reduce to $J_3(z)\equiv J(z)$ and $\ln S_3(z)\equiv \ln S(z)$. The corresponding generalization of the spectral function is

$$f_D(s)=D\frac{p^{D+3}}{(1+p^2)^2}\frac{dp}{ds} , \tag{3.9}$$

where

$$s=p^2(1+p^2)^{D/2-1} . \tag{3.10}$$

The prefactor of D in Eq. (3.9) ensures that $f_D(\infty)=1$ independently of D. The usefulness of

introducing the parameter D comes from the fact that the expressions for $\ln S_2(z)$ and $\ln S_4(z)$ are much more manageable than the one derived in the Appendix for $\ln S_3(z)$. That the cases $D=2$ and 4 bracket the case of interest, $D=3$, is established from a comparison of the spectral functions. These are exhibited in Fig. 2 by the dashed and dot-dashed curves, respectively. The $D=3$ spectral function, shown by the solid curve, is seen to be reasonably well represented by a linear interpolation between the $D=2$ and 4 curves.

B. Frequency scaling

We get an even better interpolation than the one just described by paying attention to the high-frequency asymptotes. For $z \gg 1$ we find, in analogy with Eq. (2.3),

$$\ln S_D(z) \simeq \ln(B_\infty^{(D)} z) , \tag{3.11}$$

where

$$\ln B_\infty^{(D)} = \frac{D}{2}\left[\psi\left(\frac{D}{2}+1\right)-\psi(1)\right] . \tag{3.12}$$

Here,

$$\psi(x) \equiv -\frac{d\ln\Gamma(x)}{dx} \tag{3.13}$$

is the digamma function. The specific cases of interest are

$$\ln B_\infty^{(2)} = -1 \tag{3.14a}$$

and

$$\ln B_\infty^{(4)} = -3 . \tag{3.14b}$$

As expected, Eqs. (3.14a) and (3.14b) bracket the $D=3$ result of Eq. (2.3),

$$\ln B_\infty^{(3)} \equiv \ln B_\infty = -4+3\ln 2 = -1.92 . \tag{3.15}$$

The arrows along the s axis in Fig. 2 show the effective low-frequency cutoffs at $(B_\infty^{(D)})^{-1}$ for $D=2$, 3, and 4. From Eqs. (3.14a)–(3.15) it is evident that $\ln S_D(z)$ will be a much closer approximation to $\ln S_3(z)$ if we scale the frequency by the factor

$$r_D \equiv \frac{B_\infty^{(3)}}{B_\infty^{(D)}} . \tag{3.16}$$

These factors are specifically $r_2=(2/e)^3=0.398$ and $r_4=8/e=2.94$. Defining the new approximation by

$$\ln\tilde{S}_D(z) \equiv \ln[S_D(r_D z)] , \tag{3.17}$$

we see that its high-frequency asymptote is independent of D. The corresponding spectral function is

$$\tilde{f}_D(z) = f_D(r_D z) \tag{3.18}$$

and is plotted in Fig. 3 as the dashed, solid, and dot-dashed curves for $D=2$, 3, and 4, respectively. These curves are much closer together than those for $f_D(s)$ shown in Fig. 2 and in fact cross at $z=9$. The arrow in Fig. 3 shows the effective cutoff at $z=B_\infty^{-1}=e^4/8=6.8$.

Because Eq. (3.8) in the form

$$\ln\tilde{S}_D(z) = z\int_0^\infty \frac{ds}{s}\frac{\tilde{f}_D(s)}{s+z} \tag{3.19}$$

is a linear operation on $\tilde{f}_D(s)$ we conclude that $\ln S(z)=\ln\tilde{S}_3(z)$ is also accurately given by an interpolation between $\ln\tilde{S}_2(z)$ and $\ln\tilde{S}_4(z)$. These functions are connected by Eq. (3.17) to

$$\ln S_2(z) = \left[\frac{z}{z-1}\right]^2 \ln z + \frac{z}{1-z} \tag{3.20}$$

and

$$\ln S_4(z) = \ln z - 3 - \tfrac{3}{2}\ln z + \frac{2}{z} + \frac{1}{z^2}\ln z + \left[5-\frac{5}{z}+\frac{1}{z^2}\right]R(z) , \tag{3.21}$$

where

$$R(z) = \begin{cases} \dfrac{1}{1-4z}\ln\dfrac{1+(1-4z)^{1/2}}{1-(1-4z)^{1/2}} , & 0 \le z < \frac{1}{4} \\ \dfrac{2}{(4z-1)^{1/2}}\tan^{-1}(4z-1)^{1/2} , & \frac{1}{4} \le z \end{cases} . \tag{3.22}$$

$\ln S_2$ and $\ln S_4$ vs z are plotted in Fig. 4 as the dashed and dot-dashed curves, respectively.

The manner of interpolating between $\tilde{S}_2(z)$ and $\tilde{S}_4(z)$ can be chosen by examining this low-frequency behavior, because they already agree in the high-frequency limit by virtue of the definitions of $r_{2,4}$ and as illustrated by the long-dashed line in Fig. 4. For $0<z\ll 1$ we have from Eqs. (3.8) and (3.7)

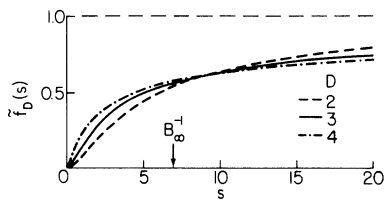

FIG. 3. Spectral function $\tilde{f}_D(s)=f_D(r_D s)$, obtained from Fig. 2 by scale changes $r_2=0.4$ and $r_4=2.9$, which bring all of the effective low-frequency cutoffs together to the same value $B_\infty^{-1}=6.8$.

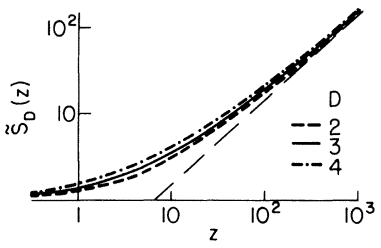

FIG. 4. Scaling function $\tilde{S}_D(z)$ vs reduced frequency $z=-i\omega/\gamma$. By scale changes all of the high-frequency asymptotes have been made to coincide, as shown by the long-dashed line. Spectral function for $\tilde{S}_D(z)$ is the $\tilde{f}_D(s)$ of Fig. 3.

$$\ln S_D = B_0^{(D)} z \ , \tag{3.23}$$

where

$$B_0^{(D)} = D \int_0^\infty \frac{dp\, p^{D-1}}{(1+p^2)^D} \ , \tag{3.24}$$

$$= \pi \frac{D}{2^D} \frac{\Gamma\left[\frac{D}{2}\right]}{\Gamma\left[\frac{D}{2}+\frac{1}{2}\right]} \ . \tag{3.25}$$

The cases of interest are $B_0^{(2)}=1$ and $B_0^{(4)}=\frac{1}{3}$, which bracket $B_0^{(3)}=B_0=\frac{3}{16}\pi=0.59$. Including the frequency scale change gives

$$\ln \tilde{S}_D = \tilde{B}_0^{(D)} z \ , \tag{3.26a}$$

where

$$\tilde{B}_0^{(D)} = r_D B_0^{(D)} \ . \tag{3.26b}$$

The numerical values are $\tilde{B}_0^{(2)}=0.40$ and $\tilde{B}_0^{(4)}=0.98$. This behavior can be understood from the following moment identity based on Eqs. (3.26a) and (3.19):

$$\tilde{B}_0^{(D)} = \int_0^\infty \frac{ds}{s^2} \tilde{f}_D(s) \ . \tag{3.27}$$

Figure 3 reveals that the D dependence of $\tilde{B}_0^{(D)}$ encountered above comes from the weighting of $\tilde{f}_D(s)$ in the small-s range, where the curves fan apart. But for $z>1$ the small-s range no longer dominates in Eq. (3.19). The crossing of the curves at $s=9$ assures that any interpolating error will be negligibly small for z in this vicinity and beyond.

In order to carry out an interpolation between $\tilde{S}_2$ and $\tilde{S}_4$ which is accurate for $z\to 0$ we give these functions the relative weights $\bar{\beta}$ and $1-\bar{\beta}$, respectively. Thus we represent S by the two-factor approximant

$$\bar{S}(z) = \tilde{S}_2^{\bar{\beta}}(z) \tilde{S}_4^{1-\bar{\beta}}(z) \ , \tag{3.28}$$

where the weighting is fixed by the low-frequency condition

$$\bar{\beta}\tilde{B}_0^{(2)} + (1-\bar{\beta})\tilde{B}_0^{(4)} = \tilde{B}_0^{(3)} = B_0 = \tfrac{3}{16}\pi \ , \tag{3.29}$$

which gives $\bar{\beta}=0.67=\frac{2}{3}$. Thus $\bar{S}=\tilde{S}_2^{2/3}\tilde{S}_4^{1/3}$, which is exhibited by the solid curve in Fig. 4. The difference between $\ln S(z)$ and the exact function $\ln S(z)$ is everywhere too small to be shown in Fig. 4. Equation (3.28) can be regarded as a definitive solution to the problem of an accurate determination of $S(z)$ in closed form.

C. Kawasaki function

In this subsection we examine an approximation which we introduced implicitly into our work at the very start. The wave-number dependence of the relaxation rate in the denominator of the integral in Eq. (2.1) has been taken to be proportional to $p^2(p^2+1)^{1/2}$. The correct expression includes the correction factor[1,2]

$$\sigma(p) = (1+p^2)^{1/2} K(p) \ , \tag{3.30}$$

where

$$K(p) = \frac{3}{4p^2}[1+p^2+(p^3-p^{-1})\tan^{-1}p] \tag{3.31}$$

is equivalent to the well-known "Kawasaki function." $\sigma(p)$ increases monotonically from its lower limit $\sigma(0)$ to its upper limit

$$\sigma_\infty \equiv \sigma(\infty) = \tfrac{3}{8}\pi = 1.178 \ . \tag{3.32}$$

The corrected version of Eq. (3.2) is

$$J(z) = 3\sigma_\infty \int_0^{q_D} \frac{dp\, p^6}{(p^2+1)^2} \times \frac{1}{z+p^2(1+p^2)^{1/2}\sigma(p)}$$
$$= 3\int_0^{q_D} \frac{dp\, p^6}{(p^2+1)^2} \times \frac{1}{\tilde{z}+(1-\rho)p^2(1+p^2)^{1/2}} \ , \tag{3.33}$$

where

$$\tilde{z} = z/\sigma_\infty \ . \tag{3.34}$$

Here we have introduced the difference function

$$\rho(p) \equiv 1 - \frac{\sigma(p)}{\sigma_\infty} \ , \tag{3.35}$$

whose limiting values are $\rho(\infty)=0$ and

$$\rho(0) = 1 - \frac{8}{3\pi} = 0.151 \ . \tag{3.36}$$

Because $\rho(p)<\rho(0)\ll 1$ for all p we can treat ρ in

Eq. (3.33) as a small first-order perturbation. Therefore we linearize with respect to ρ and proceed to calculate the effect of ρ on $J(z)$ to $O(\rho)$.

From the denominator of the integral of Eq. (3.33) we see that the relaxation rate breaks up into zeroth- and first-order terms according to

$$s(p)=s_0(p)-\Delta s(p) , \tag{3.37}$$

where $s_0(p)$ is defined by Eq. (3.3) and

$$\Delta s(p)=s_0(p)\rho(p) . \tag{3.38}$$

To find the spectral function according to Eq. (3.5) we need the derivative

$$\frac{dp}{ds}=\left[s_0'-\frac{d\Delta s}{dp}\right]^{-1}\simeq s_0'^{-1}+s_0'^{-2}\frac{d\Delta s}{dp}$$

$$\simeq s_0'^{-1}+s_0'^{-1}\frac{d\Delta s}{ds} . \tag{3.39}$$

Multiplying Eq. (3.39) by $3p^6(1+p^2)^{-2}$ gives the spectral function

$$f(s)=\frac{3}{s_0'}\frac{p^6}{(1+p^2)^2}+f_0\frac{d\Delta s}{ds}$$

$$\simeq f_0(s)+\Delta p\frac{d}{dp}\frac{3}{s_0'}\frac{p^6}{(1+p^2)^2}+f_0\frac{d\Delta s}{ds}$$

$$=f_0(s)+s_0'\Delta p\frac{df_0}{ds}+f_0\frac{d\Delta s}{ds} , \tag{3.40}$$

where in the large zeroth-order term we have allowed for the shift produced by Δs in p as a function of s. From Eq. (3.37) this shift is

$$\Delta p=\frac{\Delta s}{s_0'} , \tag{3.41}$$

which substituted into Eq. (3.40) gives the first-order spectral function change

$$\Delta f(s)=f(s)-f_0(s)=\frac{df_0\Delta s}{ds}=\frac{d(\rho sf)}{ds} , \tag{3.42}$$

where in the final expression we have substituted from Eq. (3.38) and have dropped the subscript on the zeroth-order spectral function.

The spectral function change of Eq. (3.42) determines, according to Eqs. (3.4) and (3.19), the perturbations in the high- and low-frequency parameters

$$\Delta\ln B_\infty=\int_0^\infty\frac{ds}{s}\Delta f \tag{3.43a}$$

and

$$\Delta B_0=\int_0^\infty\frac{ds}{s^2}\Delta f . \tag{3.42b}$$

Substituting Eq. (3.42) and integrating by parts gives

$$\Delta\ln B_\infty=\int_0^\infty\frac{ds}{s}\rho f=6\ln 2-4$$

$$=\ln\frac{2^6}{e^4}=\ln 1.172 \tag{3.44a}$$

and

$$\Delta B_0=2\int_0^\infty\frac{ds}{s^2}\rho f=2\langle\rho\rangle\int_0^\infty\frac{ds}{s^2}f=2\langle\rho\rangle B_0 , \tag{3.44b}$$

where the weighted mean of ρ is

$$\langle\rho\rangle\equiv\frac{\int_0^\infty\frac{ds}{s^2}\rho f}{\int_0^\infty\frac{ds}{s^2}f}=1-\frac{64}{\pi^2}\left(\tfrac{19}{18}-G\right)=0.0949 . \tag{3.44c}$$

$G=0.91597$ is Catalan's constant. Thus B_0 is changed by the factor

$$1+\frac{\Delta B_0}{B_0}=1+2\langle\rho\rangle=1.188 . \tag{3.44d}$$

The high-frequency asymptote is, from Eq. (3.44a),

$$\ln S(z)=\ln\left[\frac{2^6}{e^4}B_\infty\tilde{z}\right]=\ln\left[\frac{2^6e^{-4}}{\sigma_\infty}B_\infty z\right]$$

$$=\ln(B_\infty z) , \tag{3.45a}$$

the final form ensuing from the numerical coincidence $2^6e^{-4}=\sigma_\infty$, accurate to within 0.5%. Similarly, the low-frequency behavior is

$$\ln S(z)=\left[1+\frac{\Delta B_0}{B_0}\right]B_0\tilde{z}=\frac{1+\frac{\Delta B_0}{B_0}}{\sigma_\infty}B_0z\simeq B_0z \tag{3.45b}$$

with the final form resulting from the numerical coincidence $1+\Delta B_0/B_0=\sigma_\infty$, accurate to 1%. Added to the high-frequency shift of 0.5%, this brings the net low-frequency error to 1.5%. To this accuracy it follows from Eqs. (3.45a) and (3.45b), and as confirmed by explicit numerical computation of $\ln S$, that the Kawasaki function is adequately taken into account by the appropriate choice of variables, as defined above.

The above result can be understood by examining the spectral function change in more detail. The factor ρs which occurs in Eq. (3.42) is, like f, and thus the product ρsf, a monotonically increasing function of s. The derivative Δf is therefore a posi-

tive definite function, vanishing at the high and low ends with a maximum in the intermediate range. This can be compared with the change produced by the frequency scale change $\alpha=1+\Delta\alpha$,

$$f(\alpha s)\simeq f(s)+\Delta\alpha\,\partial_\alpha f\ , \tag{3.46}$$

where $\Delta\alpha \ll 1$ and the derivative is

$$\partial_\alpha f = sf'\ . \tag{3.47}$$

Equations (3.45a) and (3.45b) imply that Δf is canceled by $\Delta\alpha\,\partial_\alpha f$ when $\Delta\alpha=\sigma_\infty^{-1}-1=-\rho(0)$. It follows that for the reverse sign $\Delta\alpha=\rho(0)$, $\partial_\alpha f$ must be closely matched by $\Delta f/\rho(0)$.

It is straightforward to carry out the above comparison in the low- and high-frequency limits,

$$f\propto s^{5/2} \tag{3.48a}$$

and

$$1-f=\tfrac{13}{6}s^{-2/3}\ , \tag{3.48b}$$

respectively. The corresponding behavior for Eq. (3.47) is

$$\partial_\alpha f=\tfrac{5}{2}f=2.5f \tag{3.49a}$$

and

$$\partial_\alpha f=\tfrac{2}{3}(1-f)=0.67(1-f)\ . \tag{3.49b}$$

The correction from the Kawasaki function for $s\ll 1$ is

$$\frac{1}{\rho(0)}\Delta f=\frac{1}{\rho(0)}\frac{d\rho sf}{ds}\simeq\frac{dsf}{ds}=\tfrac{7}{2}f=3.5f\ . \tag{3.50a}$$

In the high-frequency range it follows from Eqs. (3.30), (3.31), and (3.35) that

$$\frac{\rho}{\rho(0)}=\frac{1}{2\rho(0)}s^{-2/3}\ . \tag{3.50b}$$

Equation (3.42) then gives

$$\begin{aligned}\frac{1}{\rho(0)}\Delta f&\simeq\frac{d}{ds}\frac{s\rho}{\rho(0)}=\frac{1}{2\rho(0)}\frac{ds^{1/3}}{ds}\\&=\frac{1}{6\rho(0)}s^{-2/3}=\frac{1}{13\rho(0)}(1-f)\\&=0.51(1-f)\ .\end{aligned} \tag{3.50c}$$

Although the coefficient in Eq. (3.49a) is somewhat smaller than that in Eq. (3.50a), and the coefficient in Eq. (3.49b) somewhat bigger than that in Eq. (3.50c), it is clear that the two functions overall match one another very well. This is the underlying reason that the effect of the Kawasaki function can be almost entirely absorbed by the frequency scale change.

We conclude this subsection by describing a second-order correction that completely removes the low-frequency error of 1.5% that we found in Eq. (3.45d). The correction is primarily of academic interest, being too small to be of practical importance. We therefore only sketch the procedure and do not provide all of the details.

The lack of precise agreement in the value B_0 is clearly associated with the imperfect overlap of the spectral functions $\Delta f/\rho(0)$ and $\partial_\alpha f$. The former's low-frequency excess and high-frequency deficiency are clearly responsible for the slightly larger value B_0, according to Eq. (3.43b). The difference of these spectral functions has a zero in the intermediate-frequency range. In Fig. 3 it is evident that the difference $\tilde{f}_4(s)-\tilde{f}_2(s)$ has the same form. We can therefore expect that the second-order correction will be well represented by

$$\Delta\ln S(z)=0.024\ln\frac{\tilde{S}_4}{\tilde{S}_2}\ , \tag{3.51}$$

where the strength has been normalized at the low-frequency end according to $\tilde{B}_0^{(4)}-\tilde{B}_0^{(2)}=0.58$.

IV. CRITICAL DIFFUSION

A. General formulation

Diffusion in a classical fluid near its critical point results from the transport of the critical fluctuations of the order parameter by the Brownian motion of the transverse shear modes.[1,2] The effect is inversely proportional to the viscosity. The appropriate average is defined further below and can be written as

$$\begin{aligned}\left\langle\frac{1}{\eta(\kappa,\omega)}\right\rangle&=\frac{1}{\eta_s(\kappa)}\langle S^{z_\eta/(3+z_\eta)}\rangle\\&\simeq\frac{1}{\eta_s(\kappa)}\left[1+\frac{z_\eta}{3}\langle\ln S\rangle\right]\ ,\end{aligned} \tag{4.1}$$

where we have substituted from Eq. (1.3). The linearization in z_η is justified by $z_\eta\ll 1$. The decrease in the effective value of the viscosity is a consequence of the retarded response of the critical fluctuations, as expressed by the frequency dependence of the viscosity. This weakening of the critical behavior can be represented by an effective correlation length $\kappa_{\rm eff}^{-1}$, smaller than κ^{-1}. Thus

$$\kappa_{\rm eff}=a_{\rm ret}\kappa\ , \tag{4.2}$$

where $a_{\rm ret}>1$ is a numerical factor of the order of unity. Substituting Eq. (4.2) into Eq. (1.1) gives

$$\frac{1}{\eta_s(\kappa_{\rm eff})}=\frac{1}{\eta_s(\kappa)}a_{\rm ret}^{z_\eta}$$
$$\simeq\frac{1}{\eta_s(\kappa)}(1+z_\eta \ln a_{\rm ret}) . \quad (4.3)$$

Identification of the factors in parentheses on the right-hand side of Eqs. (4.1) and (4.3) yields

$$\ln a_{\rm ret}=\tfrac{1}{3}\langle \ln S\rangle . \quad (4.4)$$

In this paper we confine our attention to the long-wavelength, or hydrodynamic, diffusion. In this case, p, the wave number of the transverse velocity field fluctuation, matches that of the order parameter. In addition to this "conservation of momentum" condition there is also a "conservation of energy" condition that requires a matching of ω, the velocity field frequency, to the frequency of the order-parameter fluctuation. For small values of p (this restriction is lifted in Sec. II B) this is determined by the relaxation rate $p^2D_s(\kappa)$, so that

$$\omega=ip^2D_s(\kappa) . \quad (4.5)$$

Substituting Eq. (4.5) into Eq. (1.4) and measuring p in units of κ gives

$$z=\tfrac{1}{2}p^2 . \quad (4.6)$$

To a good approximation the critical fluctuations of the order parameter contribute to the diffusion in proportion to the Ornstein-Zernike function $(p^2+1)^{-1}$. The average occurring in Eq. (4.1) is therefore defined for an arbitrary function $F(p)$ by

$$\langle F\rangle\equiv\frac{2}{\pi}\int_0^\infty\frac{dp}{p^2+1}F . \quad (4.7)$$

Our goal in this section is to determine a numerical value for $a_{\rm ret}$. As an illustration of the general ideas involved we first apply Eq. (4.7) to $\ln\bar{S}_{1,2}$, the one- and two-factor approximants of Sec. II. A more precise numerical evaluation of $\langle \ln S\rangle$ will be carried out in Sec. IV B. Substitution of Eq. (4.6) into Eqs. (2.12) and (4.7) gives

$$\ln\bar{S}_1=\ln(1+tp^2) \quad (4.8)$$

and

$$\langle \ln\bar{S}_1\rangle=\frac{2}{\pi}\int_0^\infty\frac{dp}{p^2+1}\ln(1+tp^2)$$
$$=2\sqrt{t}I(t) , \quad (4.9)$$

where

$$I(t)\equiv\frac{1}{\pi}\int_0^\infty\frac{du}{u^2+t}\ln(1+u^2) \quad (4.10)$$

and $t=\frac{1}{8}$.

Although $I(t)$ can be expressed[4] in terms of hypergeometric functions, we need it only for relatively small values of t. In this range a simple approximant gives very accurate results. First we note that

$$I(0)=1 , \quad (4.11)$$

while a subtraction yields

$$I(t)-I(0)\simeq-\tfrac{1}{2}\sqrt{t} \quad (4.12)$$

for $t\ll 1$. We therefore approximate the integral by

$$I(t)=\frac{1}{1+\frac{1}{2}\sqrt{t}} , \quad (4.13)$$

which we check at $t=1$, where it gives $\frac{2}{3}=0.667$. Exact integration yields

$$I(1)=\ln 2=0.693 , \quad (4.14)$$

indicating an error in Eq. (4.13) of 4%. As we do not need Eq. (4.13) for $t\gg 1$, the discrepancy with the exact asymptotic behavior of $\ln t/2\sqrt{t}$ that sets in in this region is of no consequence. Evaluation of Eq. (4.13) for $t=\frac{1}{8}$ and substitution into Eq. (4.9) gives for the required average

$$\langle \ln\bar{S}_1\rangle=\frac{1}{\sqrt{2}}I(\tfrac{1}{8})=\frac{1}{\sqrt{2}}\left[1+\frac{\sqrt{2}}{8}\right]^{-1}$$
$$=0.601 . \quad (4.15)$$

We now carry out the corresponding calculation for the two-factor approximant of Eq. (1.6). The logarithm breaks up into two terms, each of the form of Eq. (4.8), specified by

$$t_1=\tfrac{1}{2}B_1=1.52 \quad (4.16a)$$

and

$$t_2=\tfrac{1}{2}B_2=0.0389 \quad (4.16b)$$

and of weight $\beta=0.173$ and $1-\beta=0.827$, respectively. Thus from Eqs. (4.9) and (4.13) we obtain

$$\langle \ln\bar{S}_2\rangle=2\beta\sqrt{t_1}I(t_1)+2(1-\beta)\sqrt{t_2}I(t_2)$$
$$=0.173\times 1.53+0.827\times 0.359$$
$$=0.561 . \quad (4.17)$$

In Sec. IV B we will compare the above results obtained from $\bar{S}_{1,2}$ with the value of $\langle \ln S\rangle$ found from exact numerical evaluation.

B. Retardation correction

In Sec. IV A we obtained the retardation correction as the appropriate average over the scaling function. As an alternative way of arriving at the

same result we now interchange the order of integration and do the averaging first. Thus the average over Eq. (3.2) becomes

$$\langle J\rangle = 3\int_0^{q_D} \frac{dp\,p^6}{(p^2+1)^2}\left\langle \frac{1}{z+s}\right\rangle , \tag{4.18}$$

where $s=p^2(1+p^2)^{1/2}$ and $z=q^2/2$ according to Eqs. (3.3) and (4.6), respectively, q being the variable of integration in Eq. (4.7). Consequently, the required average in the integrand is, by Eq. (4.7),

$$\left\langle \frac{1}{z+s}\right\rangle = \frac{4}{\pi}\int_0^{\infty} \frac{dq}{(q^2+1)(q^2+2s)} = \frac{2}{\sqrt{2s}\,(1+\sqrt{2s}\,)} , \tag{4.19}$$

and in subtracted form

$$\left\langle \frac{1}{s}-\frac{1}{z+s}\right\rangle = \frac{1}{s}-\left\langle \frac{1}{z+s}\right\rangle = \frac{1}{s(1+\sqrt{2s}\,)} . \tag{4.20}$$

Substitution of Eqs. (4.20) and (3.3) into Eq. (3.1) gives the desired average value as

$$\langle \ln S\rangle = 3\int_0^{\infty} \frac{dp\,p^4}{(p^2+1)^{5/2}} \times[1+\sqrt{2}p(p^2+1)^{1/4}]^{-1} = 0.618 , \tag{4.21}$$

by numerical integration. That this result exceeds that of Eq. (4.17) by 9% is to be expected, because $\bar{S}_2$ is everywhere an underestimate of S.

The above calculation of the effect of retardation on critical diffusion is based on the hydrodynamic approximation of Eq. (4.6). This quadratic dependence on q is grossly in error for $q>1$ and goes over into a cubic dependence as $q\to\infty$. Therefore z, the dimensionless frequency ratio, approaches asymptotically a cutoff value z_c. In the notation of Perl and Ferrell[5] the corresponding cutoff value for $\ln S$ was found to be $-3\sigma(1)=0.56$. From Fig. 1 we find that this implies $z_c=2$. Defining an effective wavenumber cutoff on the hydrodynamic approximation by $z_c=q_c^2/2$ gives $q_c=2$. With the modification introduced by the cutoff, the q integration of Eq. (4.19) splits into "hydrodynamic" and "nonhydrodynamic" (NH) parts corresponding to the intervals $0\le q<q_c$, and $q_c\le q\le\infty$, respectively. For the latter interval we take $\ln S$ to have the constant cutoff value $\ln S(z_c)=0.560$, so the nonhydrodynamic part of the average is trivially

$$\langle \ln S\rangle_{\rm NH} = \frac{2}{\pi}\int_{q_c}^{\infty} \frac{dq}{q^2+1}\ln S(z_c) = 0.560\frac{2}{\pi}\tan^{-1}\frac{1}{q_c} = 0.165 . \tag{4.22}$$

Imposing the cutoff gives for the hydrodynamic part

$$\langle \ln S\rangle_H = \frac{6}{\pi}\int_0^{\infty} \frac{dp\,p^6}{(p^2+1)^2}\frac{1}{s(2s-1)} \times\left[\sqrt{2s}\,\tan^{-1}\frac{q_c}{\sqrt{2s}}-\tan^{-1}q_c\right] = 0.100 , \tag{4.23}$$

by numerical integration. The sum of Eqs. (4.22) and (4.23) yields the final value for the retardation correction,

$$\langle \ln S\rangle_{\rm ret} = 0.265 . \tag{4.24}$$

Comparison of Eqs. (4.24) and (4.21) shows that the cutoff effect has considerably reduced the effect of retardation—by more than a factor of 2. Equation (4.24) has been used by Burstyn *et al.*[6] in an analysis of the experimental light scattering linewidth data. (Note that our $\ln S$ here is three times the $\ln S$ of Burstyn *et al.*)

V. SURFACE IMPEDANCE

In this section we want to discuss the possibility of direct experimental verification of the frequency dependence of the critical viscosity $\eta_1+i\eta_2$. In Sec. IV B we showed how the frequency dependence influences the scaling function for the linewidth of the spectrum of the critical fluctuations. That is an indirect evidence of the existence of frequency dependence in the viscosity. However, a direct experimental demonstration of the effect would be desirable. Consequently, in this section we demonstrate what an experiment which measures the surface impedance of an oscillating disk or a vibrating wire in a viscous critical fluid would observe. For the binary-liquid 3-methylpentane–nitroethane we find that at a frequency of 1 kHz the effect would set in at a temperature of about 20 mK. Thus the experiment should indeed be quite feasible.

As explained in Sec. II, the measured impedance is proportional to the sum of the real and imaginary parts of the critical viscosity. In Ref. 3 we had used a logarithmic representation of the scaling function for the viscosity. In Sec. II, we found that the two-factor representation $\bar{S}_2$ is a significant improvement on the single-factor approximant and accounts for the true scaling function obtained by a numerical integration to within 15%. A more realistic simulation of the function should have a continuous spectral function rather than the one- and two-step forms implied by the one- and two-factor approximants. This motivated the approximation

$\tilde{S}_D(z)=S_D(r_D z)$. We found in Sec. III that $\tilde{S}_4$ and $\tilde{S}_2$ both give good approximations to S_3 with an error not exceeding 15%, as demonstrated in Fig. 4. In this section we will use $\tilde{S}_2$, which is slightly closer to S_3 than $\tilde{S}_4$. It furthermore has a much simpler and more convenient analytic form.

The real and imaginary parts of $\tilde{S}_2(\Omega)$ are found from Eq. (3.20) to be

$$\mathrm{Re}\ln S_2(\Omega)=\frac{\Omega^2(\Omega^2-1)}{(1+\Omega^2)^2}\ln\Omega+\frac{\pi\Omega^3}{(1+\Omega^2)^2}-\frac{\Omega^2}{1+\Omega^2}\ , \tag{5.1}$$

$$\mathrm{Im}\ln S_2(\Omega)=\frac{\pi}{2}\frac{\Omega^2(1-\Omega^2)}{(1+\Omega^2)^2}+\frac{2\Omega^3\ln\Omega}{(1+\Omega^2)^2}-\frac{\Omega}{1+\Omega^2}\ . \tag{5.2}$$

We see that $\mathrm{Re}S_2(\Omega)\sim\ln\Omega$ as the critical point is approached. Normalizing by the critical point value of the viscosity and linearizing in the small exponent z_η we find that the drop in the real part of the viscosity below its critical point value is

$$\Delta\eta_1\propto\ln(B_\infty\Omega)-\mathrm{Re}\ln\tilde{S}_2(\Omega)=\ln(B_\infty\Omega)-\mathrm{Re}\ln S_2(r_2\Omega)\ . \tag{5.3}$$

The experiment measures

$$\Delta\eta_1+\eta_2\propto H(\Omega)=\ln(B_\infty\Omega)-\mathrm{Re}\ln[S_2(r_2\Omega)]-\mathrm{Im}\ln[S_2(r_2\Omega)]\ , \tag{5.4}$$

as in Eq. (2.16). $H(\Omega)$ has been plotted as the solid curve versus

$$\Gamma=\Omega^{-1}=\gamma/\omega \tag{5.5}$$

in Fig. 5. The dashed and dot-dashed curves show separately $\ln(B_\infty\Omega)-\mathrm{Re}\ln[S_2(r_2\Omega)]$ and $-\mathrm{Im}\ln[S_2(r_2\Omega)]$, respectively. We note that apart from a change of scale these curves are very similar to the ones exhibited in Ref. 3. The change in scale comes from the difference in scale between Figs. 5 and 1 of Ref. 3. In Ref. 3 we had used the low-frequency behavior to obtain the logarithmic representation. That choice, as discussed in Sec. II, does not yield the correct asymptote in the high-frequency limit.

The arrows in Fig. 5, shown for the choice $\omega/2\pi=1$ kHz, indicate the temperatures $\Delta T=10$, 50, and 250 mK at which the characteristic relaxation rate takes on the values $\gamma/2\pi=0.046$, 0.3, and 23 kHz for the critical mixture 3-methylpentane–nitroethane. These values follow from[7] (in MHz)

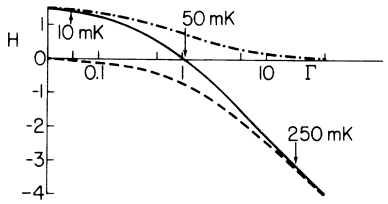

FIG. 5. Surface impedance function H of Eq. (5.2) vs the scaled rate $\Gamma=\Omega^{-1}=\gamma/\omega$. γ is the temperature-dependent characteristic relaxation rate, and ω is the frequency of the measurement. Dashed and dot-dashed curves show the separate contributions to H from the real and imaginary parts of the viscosity, respectively. Temperatures indicated are those for the binary mixture 3-methylpentane–nitroethane at the frequency of 1 kHz.

$$\frac{\gamma}{2\pi}=0.334(\Delta T)^{1.93}\ , \tag{5.6}$$

where $\Delta T=T-T_c$ is given in degrees Kelvin. The effect of the finite frequency is indicated by the deviation from the linear behavior for $\Gamma<1$. As stated before, the deviation, or "rolloff" effect, is already pronounced at $\Delta T=20$ mK. Because good temperature stability and control to within 1 mK of the critical point is generally attainable, it should be possible to map out experimentally the entire scaling function, assuming that the measurements can be carried out at 1 kHz. As noted in Ref. 3 a deviation from hydrodynamic behavior has been reported[8] for a vibrating-wire measurement of the viscosity in CO_2 near its critical point.

VI. SUMMARY

We have been concerned in this work with the frequency dependence of the critical viscosity. Because of the long-range fluctuations the viscosity of a classical fluid near the critical point is enhanced above its normal value and shows a weak divergence at $T=T_c$. This divergence is present only in the limit of vanishingly small wave number and frequency. The viscous hydrodynamic response of the fluid at a finite frequency rises as long as the frequency is small compared to the relaxation rate of the critical fluctuations. However, as one approaches T_c the fluctuations become more and more long lived and there comes a point when the relaxation rate of the fluctuations equals the external frequency. If the temperature is reduced further the system can no longer follow the rapid oscillations of the external probe, and the viscosity ceases to increase any further. This frequency dependence can be expressed by a scaling function depending only on the scaled variable $\Omega=\omega/\gamma$, where ω is the external frequency and γ is the temperature-dependent relaxation rate.

The integral which describes this frequency dependence is unfortunately rather complicated and, although exactly solvable as exhibited in the Appendix, is of little practical use. For that reason we have presented simple approximations to the true function. The simplest such approximations, corresponding to spectral functions with one and two steps, have been treated in Sec. II. In Sec. III, we develop a different approximation by varying the dimensionality of the phase space. Section IV is devoted to an application of this effect—the calculation of the diffusion coefficient in the hydrodynamic limit. The frequency dependence of the viscosity causes a small but nevertheless observable effect on the linewidth. Because of the very precise measurements of the linewidth, detection of such small effects is possible. The direct observation of the frequency dependence would, however, be more compelling. That this is indeed a feasible proposition is established in Sec. V, where we show what an experiment carried out in the binary mixture 3-methylpentane–nitroethane at 1 kHz is likely to observe as the critical point is approached.

ACKNOWLEDGMENTS

The work has been supported in part by the U. S. National Science Foundation under grants to the University of Maryland, Grant Nos. DMR-79-01172 and DMR-82-05356. We are also glad to acknowledge assistance with the computations by Mr. Michael Korth.

APPENDIX A: EXACT SCALING FUNCTION

Here we present an exact evaluation of $\ln S$. The substitution $p=\tan\theta$ reduces $\ln S$ to

$$\ln S = 3z\int_0^{\pi/2} \frac{\sin^4\theta\cos^2\theta\, d\theta}{z\cos^3\theta+\sin^2\theta} . \tag{A1}$$

The further substitution of $\cos\theta=x$ leads to

$$\ln S = 3\int_0^1 \frac{(1-x^2)^{3/2}x^2 dx}{x^3+z^{-1}(1-x^2)} . \tag{A2}$$

The denominator can be factored as

$$x^3+z^{-1}(1-x^2)=(x-\alpha_1)(x-\alpha_2)(x-\alpha_3) , \tag{A3}$$

where $\alpha_{1,2,3}$ are the roots of the cubic equation

$$x^3-z^{-1}x^2+z^{-1}=0 . \tag{A4}$$

But

$$\prod_{j=1}^{3}(x-\alpha_j)^{-1}=\sum_{i=1}^{3}\frac{A_i}{x-\alpha_i} , \tag{A5}$$

where

$$A_i=\prod_{j\neq i}(\alpha_i-\alpha_j)^{-1} . \tag{A6}$$

For any function $f(\alpha_i)$ of the three roots α_i we can write the weighted sum as the linear operation

$$\{f(\alpha)\}_A \equiv \sum_{i=1}^{3} A_i f(\alpha_i) . \tag{A7}$$

Thus by Eqs. (A5) and (A7), Eq. (A2) becomes

$$\ln S = 3\{I(\alpha)\}_A , \tag{A8}$$

where

$$I(\alpha)=\int_0^1 \frac{x^2}{x-\alpha}(1-x^2)^{3/2}dx . \tag{A9}$$

For subsequent application we note here a series of useful identities. Equation (A4) gives for $n\geq 3$ the recursion relation

$$\{\alpha^n\}_A = z^{-1}\{\alpha^{n-1}\}_A - z^{-1}\{\alpha^{n-3}\}_A . \tag{A10}$$

By direct substitution into Eq. (A7) we find

$$\{1\}_A = 0 , \tag{A11a}$$

$$\{\alpha\}_A = 0 . \tag{A11b}$$

$\{\alpha^2\}_A$ has to be computed explicitly. But from Eqs. (A10)–(A11b) it follows that all higher powers of α can be reduced to α^2. We will need

$$\{\alpha^3\}_3 = z^{-1}\{\alpha^2\}_A , \tag{A11c}$$

$$\{\alpha^4\}_A = z^{-1}\{\alpha^3\}_A = z^{-2}\{\alpha^2\}_A , \tag{A11d}$$

and

$$\{\alpha^5\}_A = z^{-1}\{\alpha^4\}_4 - z^{-1}\{\alpha^2\}_A = (z^{-3}-z^{-1})\{\alpha^2\}_A . \tag{A11e}$$

From Eqs. (A11a)–(A11e) it follows that for the polynomial

$$P(\alpha)=\sum_{n=0}^{5} a_n\alpha^n , \tag{A12}$$

$$\{P(\alpha)\}_A = [a_2+a_3z^{-1}+a_4z^{-2}+a_5(z^{-3}-z^{-1})]\{\alpha^2\}_A . \tag{A13}$$

To carry out the integration in Eq. (A9) we exhibit first the algebraic simplication of the integrand

$$(1-x^2)^{3/2}\frac{x^2}{x-\alpha} = (1-x^2)^{3/2}(x+\alpha) - \alpha^2(1-x^2)^{1/2}(x+\alpha) + \alpha^2(1-\alpha^2)\frac{(1-x^2)^{1/2}}{x+\alpha} . \tag{A14}$$

Thus

$$I(\alpha)=\tfrac{1}{5}+\tfrac{3}{16}\pi\alpha-\frac{\alpha^2}{3}-\tfrac{1}{4}\pi\alpha^3 +\alpha^2(1-\alpha^2)J(\alpha)\ , \tag{A15}$$

where

$$J(\alpha)=\int_0^1\frac{(1-x^2)^{1/2}}{x-\alpha}dx=\int_0^{\pi/2}\frac{\sin^2\theta}{\cos\theta-\alpha}d\theta$$

$$=-1-\tfrac{1}{2}\pi\alpha-(1-\alpha^2)K(\alpha) \tag{A16}$$

and

$$K(\alpha)=\int_0^{\pi/2}\frac{d\theta}{\alpha-\cos\theta} =\frac{1}{(1-\alpha^2)^{1/2}}\ln\frac{(1-\alpha)^{1/2}-(1+\alpha)^{1/2}}{(1-\alpha)^{1/2}+(1+\alpha)^{1/2}}\ . \tag{A17}$$

Substitution of Eq. (A16) into Eq. (A15) gives

$$I(\alpha)=P(\alpha)-\alpha^2(1-\alpha^2)^2K(\alpha) \tag{A18}$$

with

$$P(\alpha)=\tfrac{1}{5}+\tfrac{3}{16}\pi\alpha-\tfrac{4}{3}\alpha^2-\tfrac{3}{4}\pi\alpha^3+\alpha^4+\tfrac{1}{2}\pi\alpha^5\ . \tag{A19}$$

By Eq. (A13) the weighted sum required for Eq. (A8) is

$$\{P(\alpha)\}_A=(-\tfrac{4}{3}-\tfrac{5}{4}\pi z^{-1}+z^{-2}+\tfrac{1}{2}\pi z^{-3})\{\alpha^2\}_A\ . \tag{A20}$$

As a demonstration of the method presented above we apply it to the asymptotic region $z\gg1$. All of the roots approach zero asymptotically so the second term of Eq. (A4) can be neglected, leaving

$$x^3+z^{-1}=0\ . \tag{A21}$$

Thus

$$\alpha_i=z^{-1/3}\beta_i\ , \tag{A22}$$

where β_i are the three cube roots of -1. Because $|\alpha|\ll1$ it follows from Eq. (A17)

$$\alpha^2(1-\alpha^2)K(\alpha)\simeq\alpha^2\ln\frac{-\alpha}{2} =-(\tfrac{1}{3}\ln z+\ln2)\alpha^2 +\alpha^2\ln(-\beta)\ . \tag{A23}$$

Explicit computation yields

$$\{\alpha^2\ln(-\beta)\}_A=0 \tag{A24}$$

and

$$\{\alpha^2\}_A=1\ . \tag{A25}$$

Substituting Eqs. (A23)–(A25) into Eqs. (A16), (A15), and (A7) and neglecting all the terms in parentheses in Eq. (A20) except the first, gives finally

$$\ln S=(\ln z+3\ln2-4)\{\alpha^2\}_A=\ln(B_\infty z)\ , \tag{A26}$$

in agreement with Eqs. (2.3) and (2.4).

[1]K. Kawasaki, Ann. Phys. (N.Y.) 61, 1 (1970).
[2]R. A. Ferrell, Phys. Rev. Lett. 24, 1169 (1970).
[3]J. K. Bhattacharjee and R. A. Ferrell, Phys. Lett. 76A, 290 (1980).
[4]R. Zwanzig (private communication).
[5]R. Perl and R. A. Ferrell, Phys. Rev. Lett. 29, 51 (1972); Phys. Rev. A 6, 2358 (1972).
[6]H. Burstyn, J. V. Sengers, J. K. Bhattacharjee, and R. A. Ferrell (unpublished).
[7]H. Burstyn and J. V. Sengers, Phys. Rev. A 25, 448 (1982).
[8]L. Bruschi and M. Santini, Phys. Lett. 73A, 395 (1979).